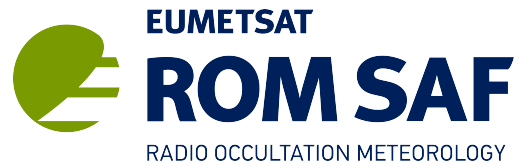


ROM SAF Report 35
Ref: SAF/ROM/METO/REP/RSR/035
Web: www.romsaf.org
Date: 11 Oct 2019



ROM SAF Report 35

An initial assessment of the quality of RO data from FY-3D

N E Bowler

Met Office, Exeter, UK

Document Author Table

	<i>Name</i>	<i>Function</i>	<i>Date</i>	<i>Comments</i>
Prepared by:	N E Bowler	ROM SAF Project Team	11 Oct 2019	
Reviewed by:	M Forsythe	Met Office review	18 Jul 2019	
Reviewed by:	J Eyre	Met Office review	25 Jul 2019	
Reviewed by:	S Healy	ROM SAF Science Coordinator	04 Oct 2019	
Approved by:	K B Lauritsen	ROM SAF Project Manager	11 Oct 2019	

Document Change Record

<i>Issue/Revision</i>	<i>Date</i>	<i>By</i>	<i>Description</i>
0.1	01 Jul 2019	NEB	1st draft
0.2	19 Jul 2019	NEB	2nd draft, following Mary's review
0.4	04 Oct 2019	NEB	3rd draft, following Sean's review
1.0	10 Oct 2019	NEB	Final version, following review by KBL

ROM SAF

The Radio Occultation Meteorology Satellite Application Facility (ROM SAF) is a decentralised processing centre under EUMETSAT which is responsible for operational processing of GRAS radio occultation (RO) data from the Metop satellites and RO data from other missions. The ROM SAF delivers bending angle, refractivity, temperature, pressure, and humidity profiles in near-real time and offline for NWP and climate users. The offline profiles are further processed into climate products consisting of gridded monthly zonal means of bending angle, refractivity, temperature, humidity, and geopotential heights together with error descriptions.

The ROM SAF also maintains the Radio Occultation Processing Package (ROPP) which contains software modules that will aid users wishing to process, quality-control and assimilate radio occultation data from any radio occultation mission into NWP and other models.

The ROM SAF Leading Entity is the Danish Meteorological Institute (DMI), with Cooperating Entities: i) European Centre for Medium-Range Weather Forecasts (ECMWF) in Reading, United Kingdom, ii) Institut D'Estudis Espacials de Catalunya (IEEC) in Barcelona, Spain, and iii) Met Office in Exeter, United Kingdom. To get access to our products or to read more about the project please go to: <http://www.romsaf.org>

Intellectual Property Rights

All intellectual property rights of the ROM SAF products belong to EUMETSAT. The use of these products is granted to every interested user, free of charge. If you wish to use these products, EUMETSAT's copyright credit must be shown by displaying the words "copyright (year) EUMETSAT" on each of the products used.

Abstract

The Feng-Yun 3D (FY-3D) satellite was launched on 14th November 2017 into a sun-synchronous polar orbit. After considerable work the data were made available via the GTS on 11th January 2019. Just under 500 occultations are provided each day, so the satellite represents an important component of the (Global Navigation Satellite System - Radio Occultation) GNSS-RO observing system. Both bending angle and refractivity measurements are made available.

Overall the quality of this data is similar to that from FY-3C. However there are two issues where the data from FY-3D is noticeably worse than that from FY-3C: a bias in setting occultations above 40km and a reduction in the number of observations below 20km. Work is being actively undertaken at the China Meteorological Administration (CMA) to address these issues. Tests have been run to assimilate bending angles from FY-3D into the Met Office system, but excluding setting occultations above 40km. These demonstrate a small but statistically significant improvement from using the data. Therefore, it is planned to include data from FY-3D into the Met Office's operational system in early 2020.

Contents

1 Bending angle evaluation	5
1.1 Bias and standard deviation characteristics	5
1.2 Vertical correlations	6
2 Refractivity assessment	10
3 Assimilation test	13
4 Other notable features	15
5 Conclusion	17

1 Bending angle evaluation

GNSS-RO data from the FY-3D satellite has been available via the Global Telecommunication System (GTS) since 11th January 2019, and performance has been stable since that date. The data in this report mainly covers the period 26th March to 26th June 2019.

1.1 Bias and standard deviation characteristics

Figure 1.1 shows the normalised difference between the bending angle observation and the background forecast from the Met Office's operational global numerical weather prediction (NWP) model. The mean and standard deviation are calculated as

$$\mu = \frac{1}{N} \sum_{i=1}^N \frac{O_i - B_i}{B_i} \quad (1.1)$$

$$\sigma = \sqrt{\frac{1}{N} \sum_{i=1}^N \left(\frac{O_i - B_i}{B_i} - \mu \right)^2} \quad (1.2)$$

where O_i and B_i are the observed and background values for occultation i in the period, and there are N occultations overall. Figure 1.1 compares the statistics of FY-3D with FY-3C and with Metop-A. Comparing with FY-3C it appears that FY-3D has a large negative bias above 45km. The Met Office model is believed to have negative bias in this region, so the positive bias with FY-3C is understood to indicate that the observations are unbiased. There is also a difference in the bias for the two satellites in the troposphere, with FY-3D appearing to have a smaller bias. Both FY-3D and FY-3C have smaller standard deviations and less bias in the troposphere than Metop-A. However, the number of valid observations starts to reduce for FY-3D below 20km, which may indicate that it is having more difficulty tracking signals in the troposphere than the other satellites.

FY-3D has slightly more observations than FY-3C over the three month period. This is due to the China Meteorological Administration (CMA) using a less strict quality control procedure for this satellite in order to allow more observations to be distributed. For FY-3C and Metop-A the number of observations is approximately constant above 10km. For FY-3D the number of observations reduces below 20km, and in the troposphere there are considerably fewer observations from FY-3D than for FY-3C. This is connected with different noise performance of the individual instruments which affects the signal tracking software (Liao Mi, personal communication).

The standard deviations are very similar for FY-3C and FY-3D. The standard deviations above 40km are slightly larger for FY-3D than for FY-3C. Both satellites have much larger standard deviations above 40km than Metop-A. This is to be expected since the Metop satellites have particularly low noise in the upper stratosphere.

The difference between rising and setting occultations is shown in Figure 1.2. This clearly shows that the large bias above 40km is due to setting occultations. This particular issue has been known for some time by CMA and is understood to be related to local multi-path effects on the setting receiver. Work is ongoing to address this and this author has seen experimental data with greatly improved characteristics. It is interesting to note that both FY satellites take more setting observations than rising - all the Metop satellites have a tendency to take more rising occultations. Standard deviations for both rising and setting occultations are larger for FY-3D above 40km. This suggests that the bias

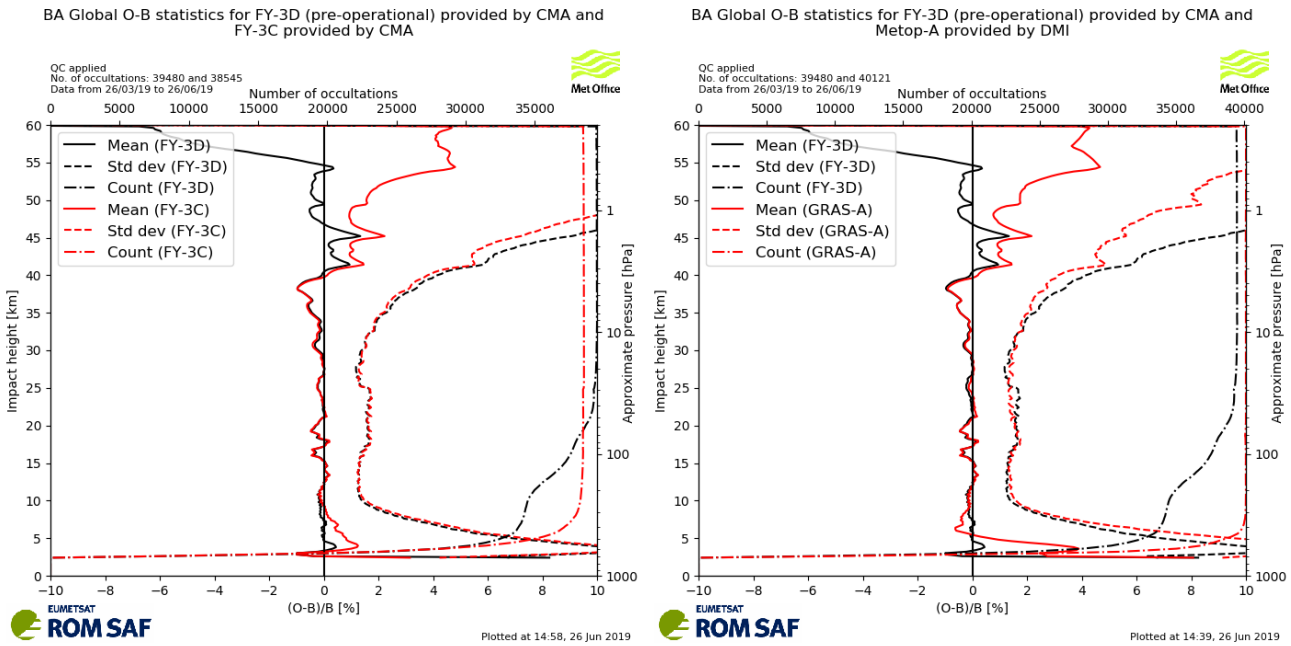


Figure 1.1: The bias and standard deviation of the normalised difference between the observation and the NWP model background forecast $(O - B)/B$ for bending angle. (left) Comparison with FY-3C and (right) Metop-A.

issue at these levels, which affects setting occultations only, is not related to the increase in standard deviations, which affects rising and setting equally. Both rising and setting occultations have a lower bias for FY-3D than FY-3C in the troposphere. The reduction in observation number below 20km mainly affects rising occultations, although the number of setting occultations reduces slightly below around 13km.

Figure 1.3 shows the bias and standard deviation, as Figure 1.1, but separated by different latitude ranges. The differences between FY-3C and FY-3D mimic the overall changes noted in the earlier figures. The one noticeable exception to this is that both satellites have a positive bias in the tropical troposphere, relative to the Met Office model. However, the bias observed for FY-3C is larger than for FY-3D, as was noted previously. In the extra-tropics the performance is very similar, indicating that the difference in performance for the troposphere for the two satellites is solely arising from the tropics. The high level bias is seen in the difference between the solid lines on each plot. However, above 55km the tropical measurements for FY-3D seem particularly biased with the mean value exceeding 10%.

1.2 Vertical correlations

When bending angle data is assimilated into the Met Office's NWP system it is assumed that the error in each bending angle measurement is independent of the errors in every other measurement. Therefore we would like the vertical observation-error covariance matrix \mathbf{R} to be diagonal, and the vertical correlations of $O - B$ (which corresponds to the covariance matrix $\mathbf{B} + \mathbf{R}$) to be close to diagonal, containing only the correlations from the background-error covariance matrix. Figure 1.4 shows the vertical correlation of the normalised difference between the observation and NWP model background forecast for FY-3D, FY-3C and Metop-A. Due to the way that bending angle is calculated as a smoothed difference between Doppler shifts, we expect a region of positive correlations near the

BA Rising/setting O-B statistics for FY-3D (pre-operational) provided by CMA and FY-3C provided by CMA

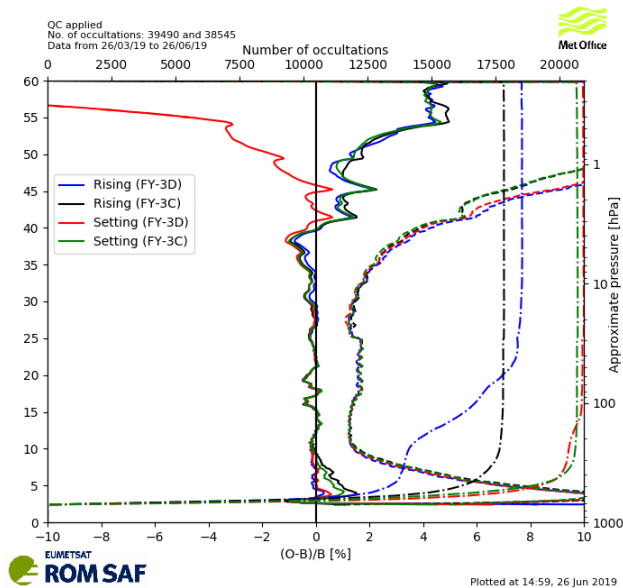
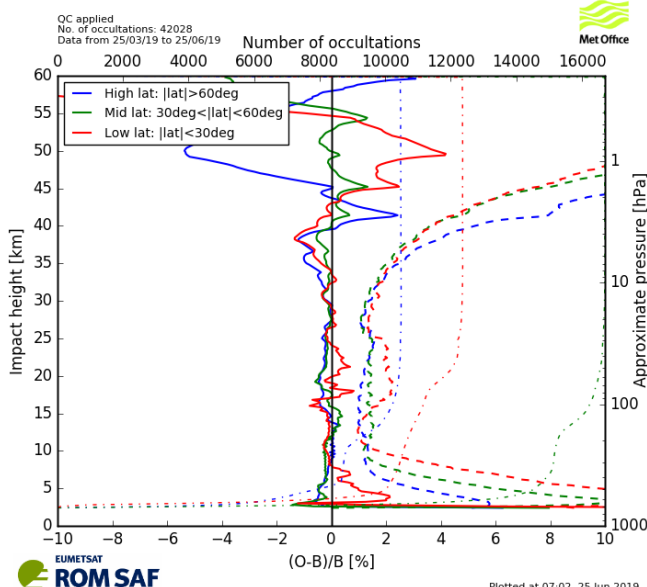


Figure 1.2: Data from rising and setting occultations, comparing FY-3D with FY-3C. The bias and standard deviation of the normalised difference between the observation and the NWP model background forecast $(O - B)/B$ for bending angle.

BA O-B statistics by latitude for FY-3D (pre-operational) provided by CMA



BA O-B statistics by latitude for FY-3C provided by CMA

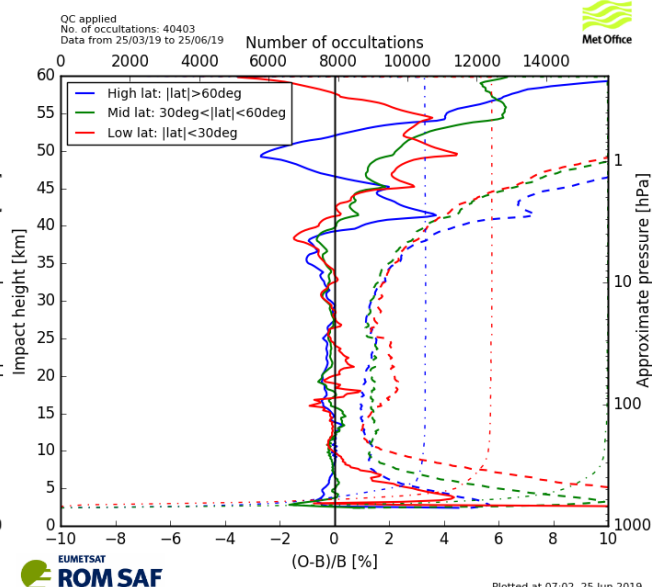


Figure 1.3: The bias and standard deviation of the normalised difference between the observation and the NWP model background forecast $(O - B)/B$, separated by different latitudes for bending angle.

diagonal, and negative correlations at further distances.

The vertical correlation patterns for FY-3D are very similar to those for FY-3C, as might be expected. Both show a sharp change in behaviour at around 26km, which is presumably the region where the processing changes from using geometric optics to wave optics. There are long-range vertical correlations towards the top of this region. Apart from this the correlation structure is similar to what would be expected, and similar to that for Metop-A. One difference is that the correlations for FY-3D and FY-3C have a slightly larger region of positive correlations above 26km, and a smaller region of negative correlations away from the diagonal compared to Metop-A. This is probably a consequence of differences in the amount of vertical smoothing that is applied to the occultations by the different processing centres.

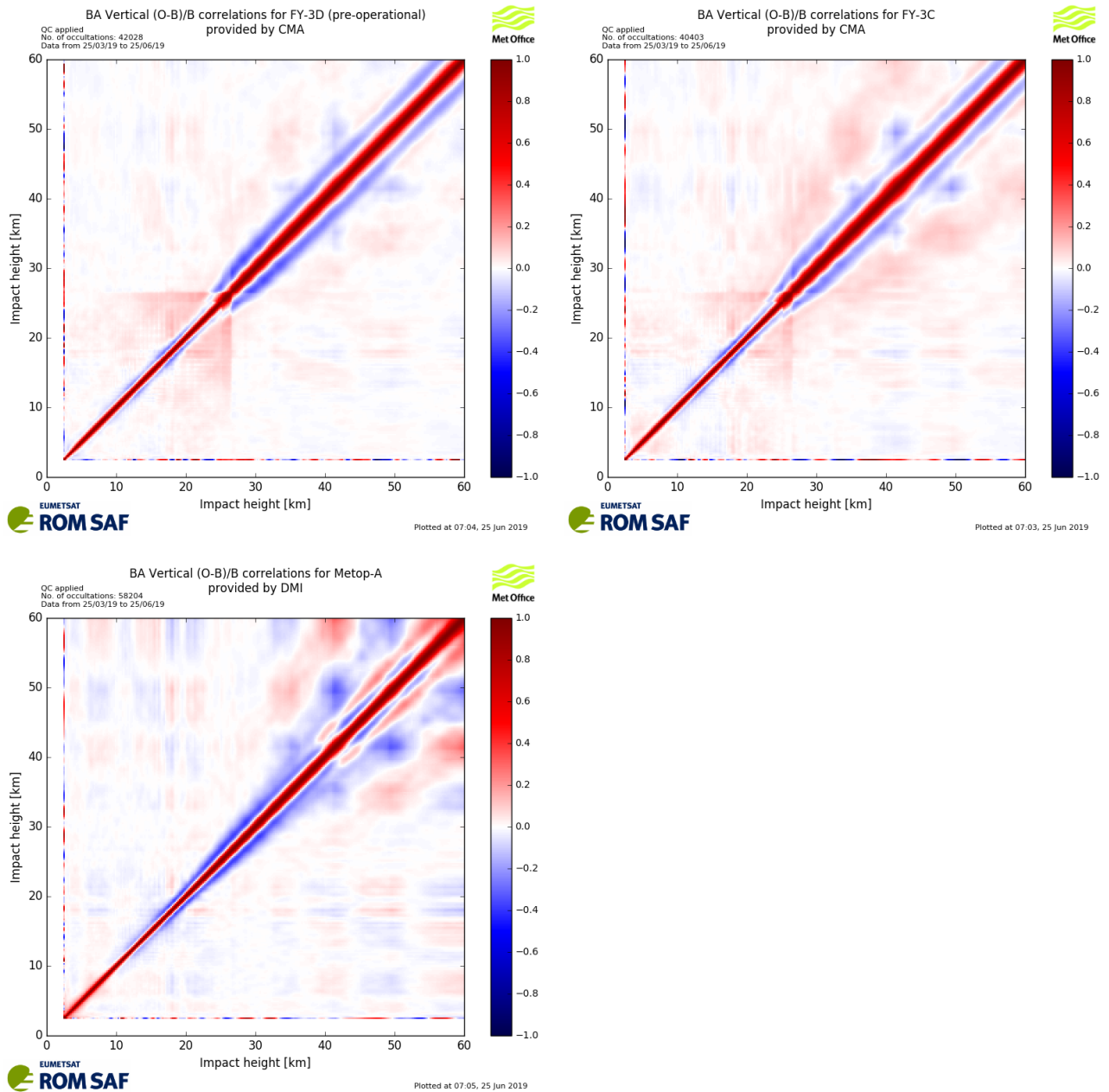


Figure 1.4: Vertical correlations of normalised differences between the observation and the NWP model background for bending angle.

2 Refractivity assessment

Measurements of refractivity are calculated from the bending angle by CMA. Figure 2.1 shows the mean and standard deviation of normalised differences between the observed refractivity and that produced by the NWP model forecast. Note that due to problems with the plotting, this is for a slightly different date than the other figures. The comparison with FY-3C shows many of the same features that were seen for the bending angle assessment. The different (smaller in this case) bias above 40km, the increased standard deviation above 45km, the reduction in the number of observations below 20km, and the reduced bias in the troposphere. Additionally, the refractivity shows a smaller standard deviation for FY-3D between 25 and 40km, which is not seen for bending angles. It is not clear why this slightly different behaviour is seen.

The vertical correlation of the difference between modelled and observed refractivity are shown in Figure 2.2 for FY-3D, FY-3C and Metop-A. The FY satellites are very similar to each other and have longer vertical correlations than Metop-A. This may be a consequence of different choices around vertical smoothing in the processing by the different centres.

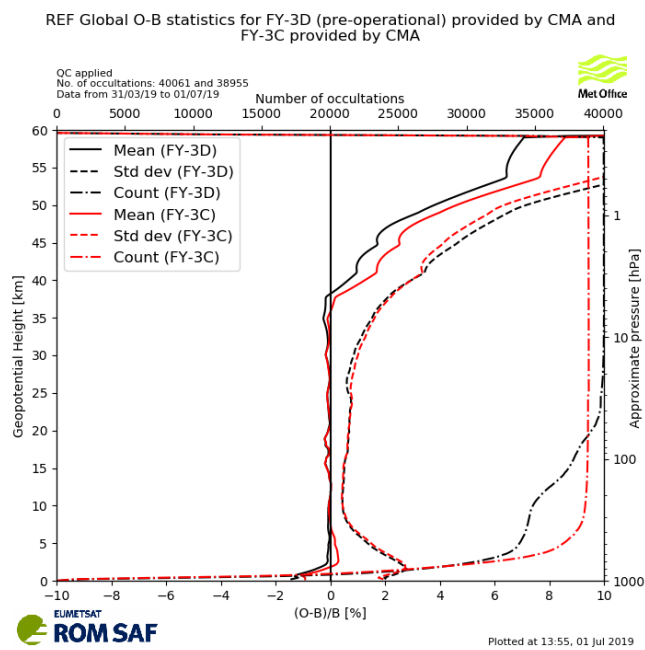


Figure 2.1: The bias and standard deviation of the normalised difference between the observation and the NWP model background forecast $(O - B)/B$ for refractivity.

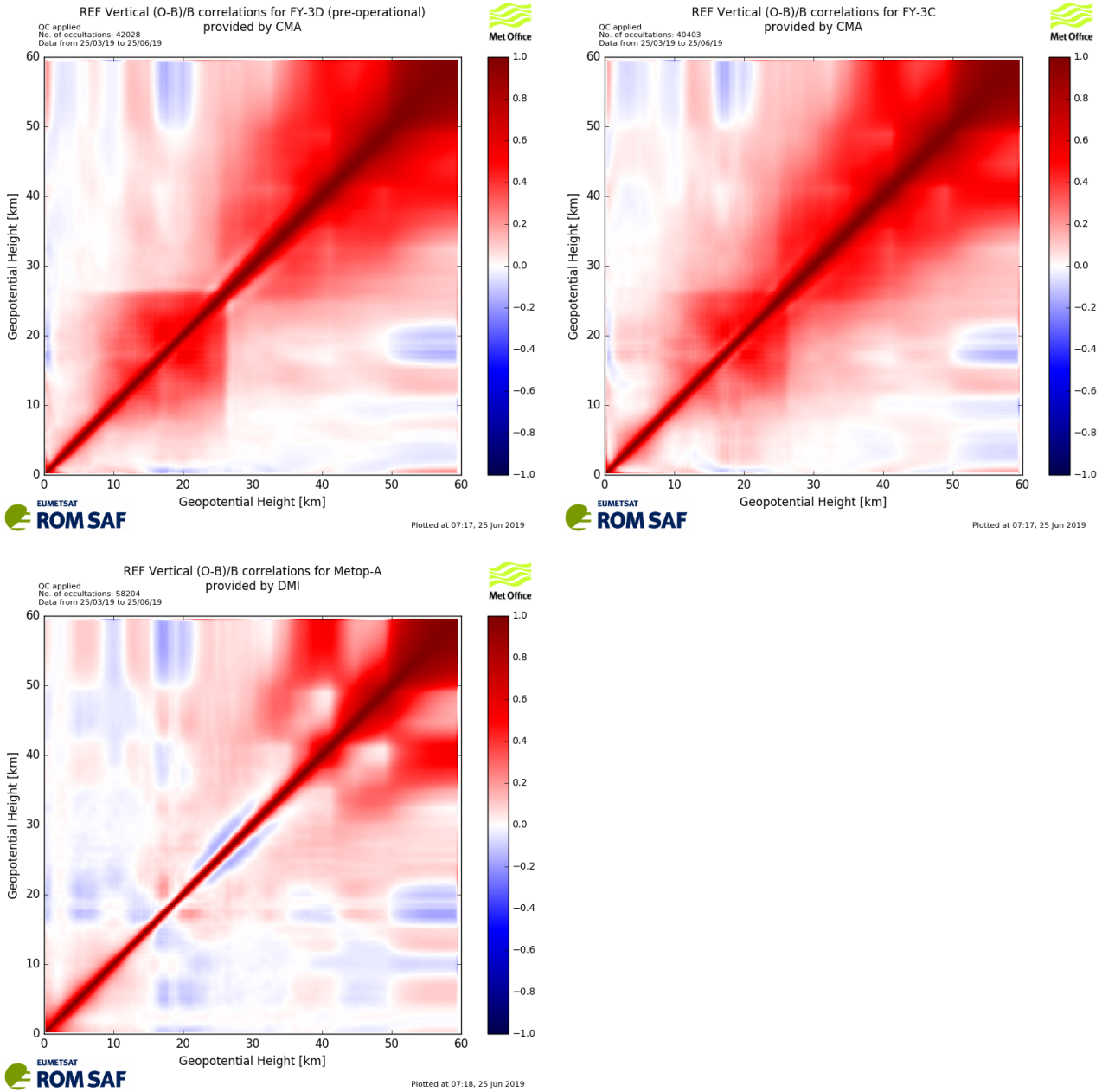


Figure 2.2: Vertical correlations of normalised differences between the observation and the NWP model background for refractivity.

3 Assimilation test

In order to test the impact that adding these data would have on the operational NWP system an assimilation test was run. This test mimics the operational system at low resolution, adding bending angle observations from FY-3D to the data assimilation. Setting observations above 40km were excluded, given the bias noted previously. This is compared with a similar low-resolution run without the additional observations. The test was run between 15th January and 15th April 2019 using a global forecast model at N320 resolution (640x480 grid-points). 7-day forecasts are launched every 12h, and these are verified against ECMWF analyses and against observations. Verification results are shown in Figure 3.1. These show that the forecasts which include FY-3D observations have smaller errors for many variables. The change appears to be particularly beneficial when verifying against ECMWF analyses. There are no variables for which there is a clear degradation in performance.

When assessing forecast performance, we also consider assimilation statistics. This is the root-mean-square (RMS) difference between the forecast from the previous data assimilation cycle (6h ago) and the observations. The change in the RMS difference to satellite sounding channels (microwave and infra-red) provides useful information on the behaviour of the assimilation with the new observations. For this test the change in the RMS difference is generally neutral (with some channels showing a larger RMS difference and some showing a smaller RMS).

% Difference (Add FY-3D (restrict setting below 40km) vs.
Control) - overall 0.14%
RMSE against ecanal for 20190115 to 20190415

% Difference (Add FY-3D (restrict setting below 40km) vs.
Control) - overall 0.1%
RMSE against observations for 20190115 to 20190415

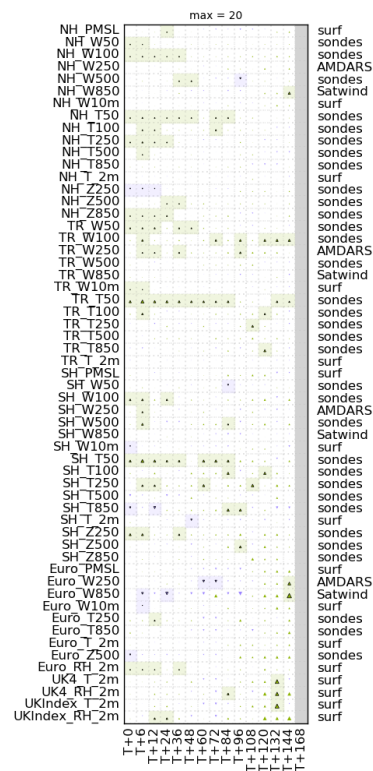
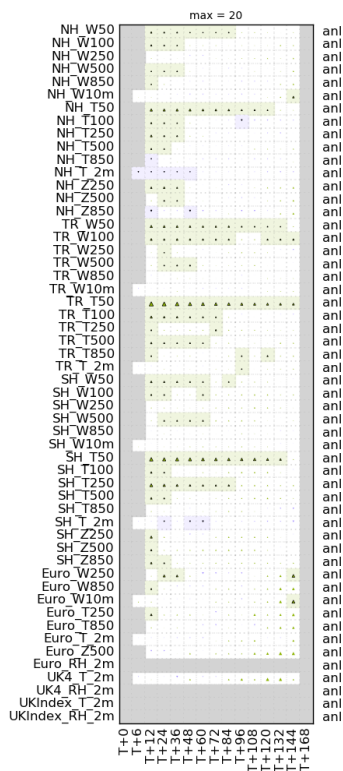


Figure 3.1: Verification results for a test using observations with FY-3D, compared to a baseline system. (left) Verification against ECMWF analyses and (right) verification against observations. The triangles show the change in the root-mean-square (RMS) error of the forecast, with green (blue) triangles indicating that the test has smaller (larger) errors. Where the change is statistically significant the box surrounding the triangle is shaded.

4 Other notable features

The timeliness of the data, as received via GTS is shown in Figure 4.1. 90% of the observations are received in 4 hours and 39 minutes, which is slightly slower than FY-3C (4 hours and 18 minutes) and much slower than Metop-A (2 hours). The “main” run of the Met Office forecast system takes place at around 2 hours and 40 minutes after the nominal time of the data assimilation window. Observations which are delayed are less likely to be available in time to be used in this run. We estimate that approximately 50% of observations from FY-3D will be used by the “main” run, compared with around 52% for FY-3C and 65% for Metop-A. The NWP also has an “update” run which is run around six hours after the nominal time. Many more observations from all satellites are used in this assimilation.

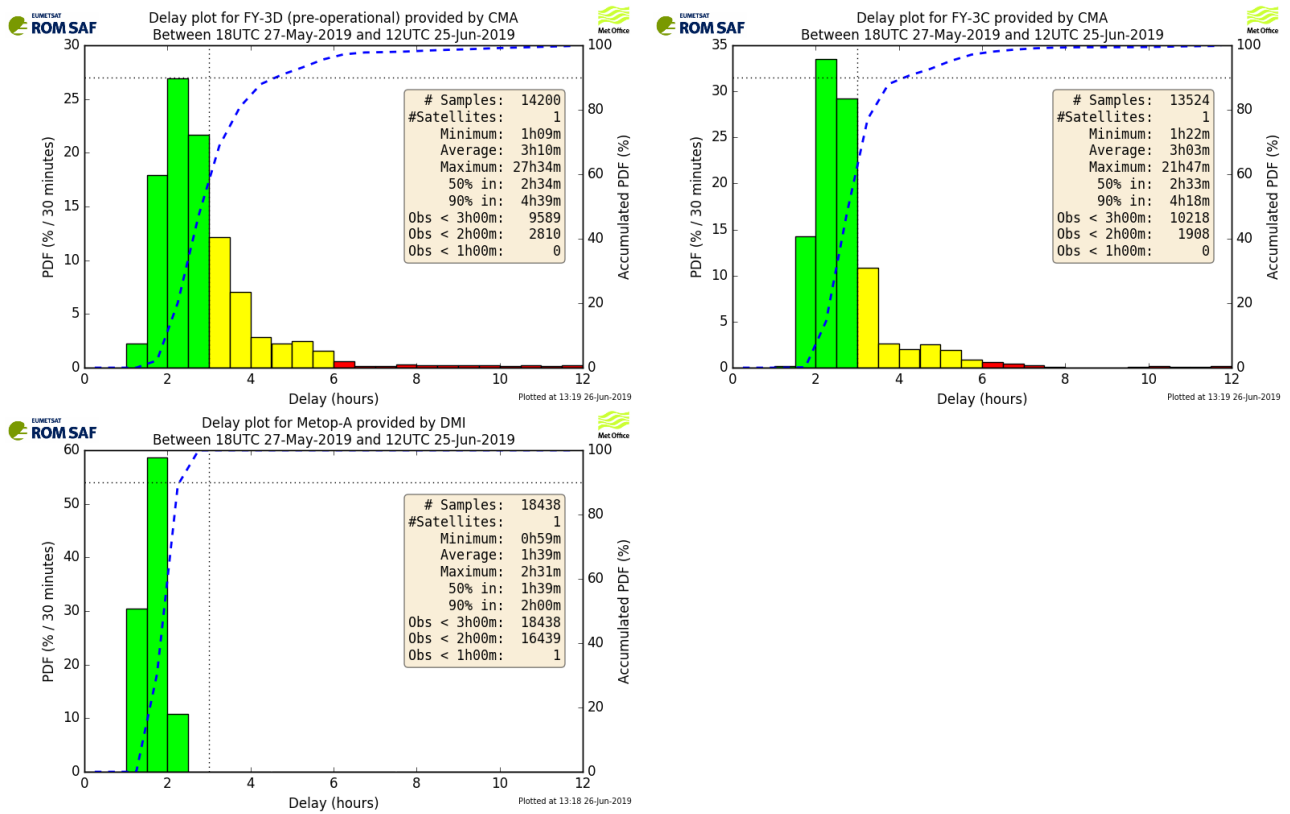


Figure 4.1: Time delay in receiving the occultations, as calculated from the receipt time in the Met Office’s observations data base.

5 Conclusion

The overall quality of the data from FY-3D is similar to that from FY-3C, as might be expected. Notable differences are

- Setting bending angles above 40km show a negative bias, compared to other observations.
- Below 20km the number of observations reduces, particularly for rising occultations.
- The standard deviation of the observations (relative to Met Office background forecasts) is slightly larger than for FY-3C above 45km.
- In the tropical troposphere FY-3D has a smaller bias (relative to Met Office background forecasts) than FY-3C.
- Both FY-3D and FY-3C have increased standard deviations and larger vertical correlations between 18 and 25km, relative to heights above and below this range. It is assumed that this is related to the transition between the use of geometric optics and wave optics in the processing.

Tests using bending angle observations from FY-3D in the Met Office assimilation system have been conducted, excluding setting occultations above 40km. These show a benefit from the introduction of this data, and it is intended to use this data operationally in early 2020.

ROM SAF (and earlier GRAS SAF) Reports

SAF/GRAS/METO/REP/GSR/001	Mono-dimensional thinning for GPS Radio Occultation
SAF/GRAS/METO/REP/GSR/002	Geodesy calculations in ROPP
SAF/GRAS/METO/REP/GSR/003	ROPP minimiser - minROPP
SAF/GRAS/METO/REP/GSR/004	Error function calculation in ROPP
SAF/GRAS/METO/REP/GSR/005	Refractivity calculations in ROPP
SAF/GRAS/METO/REP/GSR/006	Levenberg-Marquardt minimisation in ROPP
SAF/GRAS/METO/REP/GSR/007	Abel integral calculations in ROPP
SAF/GRAS/METO/REP/GSR/008	ROPP thinner algorithm
SAF/GRAS/METO/REP/GSR/009	Refractivity coefficients used in the assimilation of GPS radio occultation measurements
SAF/GRAS/METO/REP/GSR/010	Latitudinal Binning and Area-Weighted Averaging of Irregularly Distributed Radio Occultation Data
SAF/GRAS/METO/REP/GSR/011	ROPP 1dVar validation
SAF/GRAS/METO/REP/GSR/012	Assimilation of Global Positioning System Radio Occultation Data in the ECMWF ERA-Interim Re-analysis
SAF/GRAS/METO/REP/GSR/013	ROPP PP validation
SAF/ROM/METO/REP/RSR/014	A review of the geodesy calculations in ROPP
SAF/ROM/METO/REP/RSR/015	Improvements to the ROPP refractivity and bending angle operators
SAF/ROM/METO/REP/RSR/016	Simplifying EGM96 undulation calculations in ROPP
SAF/ROM/METO/REP/RSR/017	Simulation of L1 and L2 bending angles with a model ionosphere
SAF/ROM/METO/REP/RSR/018	Single Frequency Radio Occultation Retrievals: Impact on Numerical Weather Prediction
SAF/ROM/METO/REP/RSR/019	Implementation of the ROPP two-dimensional bending angle observation operator in an NWP system
SAF/ROM/METO/REP/RSR/020	Interpolation artefact in ECMWF monthly standard deviation plots
SAF/ROM/METO/REP/RSR/021	5th ROM SAF User Workshop on Applications of GPS radio occultation measurements
SAF/ROM/METO/REP/RSR/022	The use of the GPS radio occultation reflection flag for NWP applications
SAF/ROM/METO/REP/RSR/023	Assessment of a potential reflection flag product
SAF/ROM/METO/REP/RSR/024	The calculation of planetary boundary layer heights in ROPP
SAF/ROM/METO/REP/RSR/025	Survey on user requirements for potential ionospheric products from EPS-SG radio occultation measurements

ROM SAF (and earlier GRAS SAF) Reports (cont.)

- SAF/ROM/METO/REP/RSR/026 Estimates of GNSS radio occultation bending angle and refractivity error statistics
- SAF/ROM/METO/REP/RSR/027 Recent forecast impact experiments with GPS radio occultation measurements
- SAF/ROM/METO/REP/RSR/028 Description of wave optics modelling in ROPP-9 and suggested improvements for ROPP-9.1
- SAF/ROM/METO/REP/RSR/029 Testing reprocessed GPS radio occultation datasets in a reanalysis system
- SAF/ROM/METO/REP/RSR/030 A first look at the feasibility of assimilating single and dual frequency bending angles
- SAF/ROM/METO/REP/RSR/032 An initial assessment of the quality of RO data from KOMPSAT-5
- SAF/ROM/METO/REP/RSR/033 Some science changes in ROPP-9.1

ROM SAF Reports are accessible via the ROM SAF website: <http://www.romsaf.org>